Silica/polystyrene bipod-like submicron colloids synthesized by seed-growth dispersion polymerisation as precursors for two-patch silica particles

Sharvina Shanmugathasan, Auriane Bagur, Étienne Ducrot, Sonia Buffiere, Peter van Oostrum, Serge Ravaine, Etienne Duguet

Silica/polystyrene bipod-like submicron colloids synthesized by seed-growth dispersion polymerisation as precursors for two-patch silica particles

Sharvina Shanmugathasan[a,b], Auriane Bagur[a,b], Etienne Ducrot[a], Sonia Buffière[b], Peter van Oostrum[c], Serge Ravaine[a]* and Etienne Duguet[b]*

[a] Univ. Bordeaux, CNRS, CRPP, 33600 Pessac, France. serge.ravaine@crpp.cnrs.fr

[b] Univ. Bordeaux, CNRS, Bordeaux INP, ICMCB, 33600 Pessac, France. etienne.duguet@icmcb.cnrs.fr

[c] University of Natural Resources and Life Sciences, Department of Nanobiotechnology, Institute for Biologically Inspired Materials, Muthgasse 11-II, A-1090, Vienna, Austria.
peter.van.oostrum@boku.ac.at

Abstract

We report the synthesis at the gram scale of spherical silica particles bearing two organic patches made of grafted polystyrene chains at their poles. The patchy character of the particles is evidenced by combining transmission electron microscopy analysis and electron energy-loss spectroscopy. The multi-stage synthesis is based on the fabrication of silica/polystyrene bipods by dispersion polymerisation followed by the selective dissolution of the polymeric nodules, and leads to about 70% pure batches. The morphological purity is increased up to 98% by flow cytometry experiments. The polyethylenimine used as a stabiliser in the polymerisation step seems to play an important role in the detection of patches since the latter proved unsuccessful for particles obtained in the presence of polyvinylpyrrolidone.

Keywords

Two-patch silica particle; Seed-growth dispersion polymerisation; Bipod-like silica/polystyrene particle; Electron microscopy; Electron energy-loss spectroscopy; Flow cytometry

1. Introduction

Patchy particles, which are particles having a zone of different chemical nature or topology, are good candidates as building units to fabricate new colloidal structures with photonic or catalytic properties by self-assembly [1,2]. In particular, two-patch particles have been assembled into colloidal clusters [3], linear chains [4–6] or two-dimensional lattices [7].

Several synthetic strategies of two-patch particles have been successfully developed in recent years. For example, Kretzschmar and Pawar used the glancing angle deposition method to create two patches oppositely positioned on spherical micrometric particles previously organized in a close-packed monolayer [8]. van Oostrum *et al.* have used a polystyrene (PS) membrane as a temporary mask to synthesize silica microparticles with two polar patchs at the surface of an agarose gel [9]. Zimmerman *et al.* fabricated silica particles with two polar patches by microcontact printing with polyethyleneimine (PEI) ink and poly(dimethoxysilane) stamps [10].

One of the main drawbacks of the above strategies based on the use of a two-dimensional template is the low amount of produced particles per batch, which is a severe limitation for further applications. To overpass this limitation, several strategies based on the use of 3D colloidal crystals, emulsion droplets or larger particles as scaffolds, which provide a higher amount of surface area per unit volume, have been developed to fabricate patchy particles in a higher yield [1,2]. Patchy gold nanorods have been produced by Kumacheva *et al.*, who took advantage of the presence of {111} facets specifically at both ends of gold nanorods to graft thiol-ended PS macromolecules only there [4]. We have reported the synthesis of silica/PS bipods by emulsion polymerisation of styrene in the presence of silica particles of a few tens of nanometres [5,6]. The exceptional morphological yield of 97% has allowed the fabrication of quasi-pure batches of 2-patch silica particles by dissolution of the nodules of so-called bipods and thus to perform self-assembly studies. To develop two-patch particles of several hundred nanometres, emulsion polymerisation proves unsuitable, as PS nodules cannot exceed 300 nm in diameter and lead to "raspberry" morphologies under these conditions [11]. To obtain regular bipods, *i.e.* where the PS nodules are aligned with the central seed, it is essential that the two PS nodules can reach sizes much larger than the seed to be able to move away from each other as much as possible for steric - and possibly electrosteric - reasons during their growth. Obtaining large PS nodules thus requires the use of another polymerisation process, which is dispersion polymerisation. This differs from emulsion polymerisation in that the monomer is soluble in the reaction medium and the latex particles formed are not stabilised by a surfactant but by homopolymers such as polyvinylpyrolidone (PVP), polyvinyl alcohol or hydroxycellulose. Very marginally, Hong *et al.* have shown that it is also possible to use PEI [12].

Previous work has described the use of silica particles in the dispersion polymerisation of styrene. Some have used colloidal silica as a stabiliser and obtained raspberry morphologies where PS particles are coated with inorganic nanoparticles [13–16]. Others have pre-modified the surface of the silica particles to encapsulate them in the polymer and obtain core-shell particles or composite particles [17–22]. Some of these works have shown that, in ethanol and in the presence of the stabiliser PVP, surface-modified silica particles of sufficient size can serve as seeds for latex growth and lead to multipod particles [19–22]. The authors of these studies point out that the number of nodules per seed decreases during growth, but in an uncontrolled manner leading to a high polydispersity in the number, position and size of PS nodules. Among these multipods, the authors observed quite well-shaped bipods, but no statistical study was conducted [21,22].

We were inspired by these works to develop a protocol using PEI as a stabiliser and allowing to obtain silica/PS bipods with a morphological yield of around 70%. This paper presents this protocol and our efforts to reveal the two patches made of grafted PS macromolecules obtained after dissolution of the two PS nodules. We also show that it is possible to increase drastically the morphological yield by using a technique known as flow cytometry cell sorting [23] to sort the bipods by the amount of light they scatter. Our experimental approach is summarized in Figure 1.

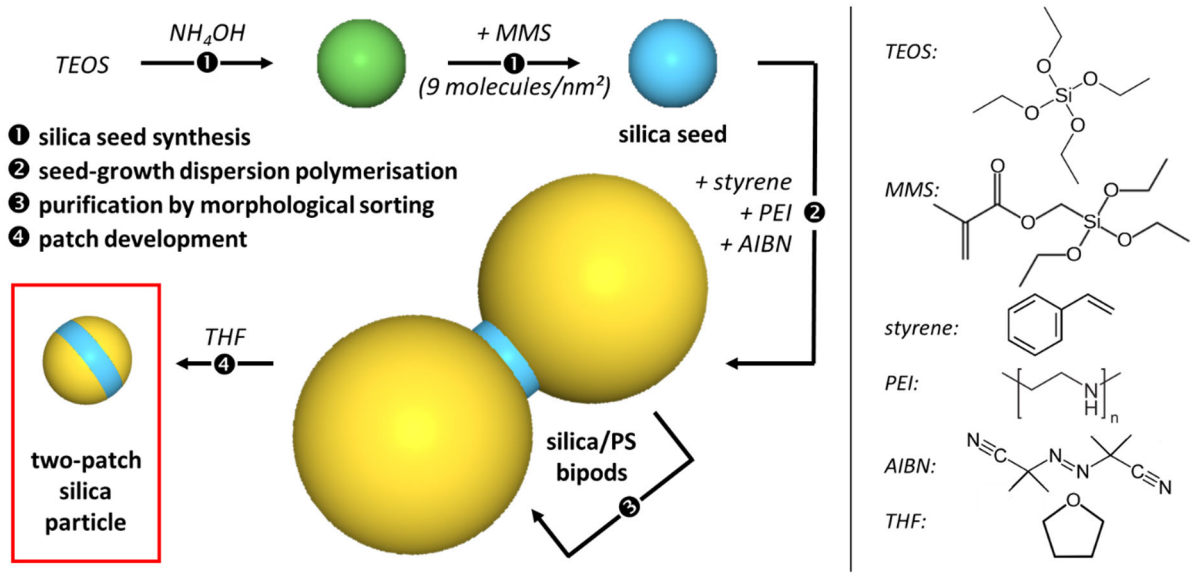

Figure 1: Synthetic pathway and chemical formula of the reagents used for the synthesis of 2-patch silica particles.

2. Materials and methods

2.1 Materials.

Tetraethoxysilane (TEOS, Fluka) and ammonia (28-32% in water, J.T. Baker) were purchased in their reagent grades and used without further purification. Styrene (99%, Aldrich), methacryloxymethyltriethoxysilane (MMS, ABCR), azobis (isobutyronitrile) (AIBN, Acros), absolute ethanol (VMR) and branched polyethyleneimine (PEI, M_w~70,000 g.mol^{-1}, Alfa Aeser), Nile Red (Thermo Fisher), Triton^{TM} X-100 (Sigma Aldrich) and tetrahydrofuran (THF, Sigma Aldrich) were used as received. Deionized water with a resistivity of 18.2 MΩ.cm at 25 °C was obtained with a Milli-Q system (Millipore).

2.2 Synthesis and surface functionalisation of silica seeds.

Silica particles with a mean diameter of 500 ± 19 nm were prepared as follows: in a 500-mL round flask maintained at 18°C, 100 mL of absolute ethanol and 20 mL of an aqueous solution of ammonia were introduced and stirred at 400 rpm to homogenise. 45 mL of diluted TEOS (20 vol% in absolute ethanol) were then introduced dropwise at an addition rate of 8.1 mL.h^{-1}, and the solution was left under stirring for 8 h. After evaporation of three quarters of the liquid phase using a rotary evaporator, the seeds were washed by three centrifugation/redispersion cycles in absolute ethanol (12,000 g, 5 min).

The surface of the silica seeds was then functionalised through the chemical grafting of MMS as follows: 100 mL of the silica seeds suspension (10 g/L) were poured in a round flask of 250 mL together with 20 mL of an aqueous solution of ammonia and the solution was stirred at 700 rpm to homogenise. The calculated amount of MMS corresponding to a nominal surface density of 9 molecules/nm^2 (assuming perfect sphericity of the particles and their non-porosity) was added into the solution and the mixture was stirred at 300 rpm for 3 h at room temperature and then at 90 °C for 1 h. Then, the seeds were washed as previously described. The silica seed suspension was concentrated, and its final concentration of 52.4 g/L was determined by measuring the mass of a dried extract.

2.3 Synthesis of silica/PS bipods by seed-growth dispersion polymerization of styrene. PEI (250 mg) was dissolved into 50 mL of the reaction medium made of 4.2 mL of the previous silica seed dispersion, 5 mL of styrene and 40.8 mL of absolute ethanol. This dispersion was poured in a 100-mL reactor fitted with a condenser and deaerated by bubbling nitrogen for 2 h. In parallel, 25 mg of AIBN were dissolved in 2.5 mL of absolute ethanol and the solution was deaerated in the same conditions. Then, the temperature was raised to 75°C, while the stirring speed was set at 350 rpm. Lastly, the AIBN solution was added and the polymerisation reaction was carried out for 6 h. The particles were washed by three centrifugation/redispersion cycles in absolute ethanol (12,000 g, 5 min). The concentration of the final dispersion was 65 g/L.

2.4 Dissolution of the PS nodules. The suspension of bipods (1 mL) was diluted 20 times in absolute ethanol and centrifuged (12,000 g, 5 min). The pellet was redispersed in THF (40 mL) and the non-grafted PS chains were removed by three centrifugation/redispersion cycles in THF (12,000 g, 5 min, 40 mL). The final pellet was redispersed in absolute ethanol.

2.5 Staining of the hydrophobic areas of the silica/PS bipods with Nile red. The silica/PS bipods (100 µL) were incubated with Nile red in ethanol (400 µL) for at least 2 h. Then 500 µL of water were added to force the Nile red to label the hydrophobic parts and the dispersion turned from pink to purple. The particles were observed under a Zeiss LSM 980 confocal microscope (oil immersion objective x 63) at an excitation wavelength of 488 nm.

2.6 Characterization and purification of the bipod batches. The dispersion of bipods (175 µl) was diluted in 50 mL of aqueous solution of Triton™ X-100 (1 vol.%). The tube was introduced into the sampling compartment of the flow cytometer (Beckman Coulter MoFlo Astrios EQ) and analysed at a wavelength of 488 nm. Cytometry in general strives to provide information on individual cells, or in this work particles [23]. The liquid containing the objects of interest is diluted with a buffer designed to achieve a certain viscosity and surface tension such that a jet of the final mixture breaks apart into reproducible droplets. At sufficient dilution such that the objects pass a series of detectors individually, the information can be combined on the individual object level. This allows the identification of sub-populations in the sample. For biological or medical examinations of cells, fluorescent labels that specifically bind to particular molecules such as proteins are typically used. The information obtained with the cytometer is then the relative amounts of the different labels and correlations between these. In addition to fluorescence assays, it is possible to collect information on the light scattering, which does not provide information on molecular details but rather on geometrical parameters such as size, shape and refractive index distribution. In the flow cytometer used in this work, the light scattering is measured in the forward and the sideward direction. This is a very crude approximation of the information one can collect with static light scattering, but importantly on a per particle level rather than on a population average level. The intensity of the scattered light in the two directions is continuously measured and any peaks in this signal are used to identify the passage of an object and to characterize it. The peaks are quantified in two ways in the software: by specifying the highest brightness that was observed during the passage and by providing an integral measure of all the light that was scattered and collected as it passed by. The latter is referred to as “area of the forward/sideward scattered light” (denoted as 488-FSC1-Area and 488-SSC-Area) as it quantifies the area under the peak in the intensity/time graph. We found that the best discriminatory results were obtained by plotting the area of the forward scattered light against that of the sideward scattered light. Finally, it is possible to sort the objects based on combinations of the individual objects’ measurements. This is done by electrically charging a jet of the flow with the characterized objects that then breaks up into droplets. The charge helps to break the flow up into droplets. The train of charged droplets is deviated as it falls by applying an electric field that directs it to one of several

containers. If the sorting criteria are properly chosen and the dilution is sufficient to provide enough time and empty droplets between two differently identified objects, it is thus possible to sort them. The recovery of particles was performed in five sorting tubes, corresponding to the fractions indicated by black ellipses in Figure 4.

2.7 Characterisation techniques. Transmission Electron Microscopy (TEM) experiments were performed with a Hitachi H600 microscope operating at an acceleration voltage of 75 kV. The samples were prepared as follows: the colloidal dispersion, as directly collected from the reactor, was diluted in ethanol. Ten drops were deposited on a copper grid coated with a carbon membrane and the liquid was left to evaporate at room temperature. Scanning electron microscopy (SEM) analyses were performed on a Hitachi SEM T-1000 microscope operating at 15 kV and on a Apreo VS SEM (Thermo Scientific, Eindhoven, The Netherlands) operating at 1 to 5 kV (Vienna). In preparation for inspection using the Hitachi SEM T-1000, a thin layer of Gold-Palladium alloy was sputtered onto samples during 60 s before analysis. Confocal microscopy experiments were performed with a Zeiss LSM 980 microscope with an oil immersion objective (x 63). Particles were examined by electron energy-loss spectroscopy (EELS) with a JEOL JEM 2200FS equipped with an "Omega-in-column" energy filter. The colloidal solution was diluted in ethanol, and ten drops of the diluted suspension was deposited on a copper grid coated with a carbon membrane with holes. For size exclusion chromatography (SEC) experiments, we collected, dried, weighed the first THF supernatant containing the dissolved PS chains, and then dissolved it again in analytical grade THF at a mass concentration of 5 mg/mL. Experiments were performed in THF with a Wyatt Technology setup using 0.2 vol% of trichlorobenzene as standard.

3. Results and discussion

3.1 Synthesis of silica/PS bipod-like particles

The batch of silica spherical particles used in this study was obtained by hydrolysis/condensation catalysed by ammonia in hydro-alcoholic medium where tetraethyl orthosilicate (TEOS) was continuously added [21]. The particles had an average diameter of 500 nm and a polydispersity index Dw/Dn = 1.03. They were then surface modified by hydrolysis/polycondensation of methacryloxymethyltriethoxysilane (MMS) at a nominal surface grafting density of 9 molecules/nm^2, corresponding to a highly cross-linked polysiloxane film a few atoms thick [24]. The methacryloxymethyl pendant groups are mainly exposed to the outside, giving the particles an organophilic character to promote the nucleation/growth of PS nodules and also allowing the covalent anchoring of the closest macromolecules by copolymerisation with the methacrylate moieties.

The seed-growth polymerisation of styrene was carried out according to a procedure already reported [20,21] with two differences: the stabiliser PVP was replaced by PEI and the styrene was introduced into the reactor at the beginning of the protocol, as proposed by other authors [22]. After adjusting various parameters such as the concentrations of the different reagents, the temperature and the duration of the experiment, we arrived at operating conditions optimised for 500 nm silica seeds, described in the experimental section. The prepared batches were observed by transmission (Figure 2A) and scanning electron microscopy (Figure 2B) and their morphological purity was calculated by statistical analysis of 300 silica-containing particles, which means that possible free latex particles, i.e. not bound to the silica seeds, were not included in the statistics. The results showed that 69% of the hybrid objects are undoubtedly bipods. The two PS nodules are in general aligned with the silica seed (two extreme examples are given in the insets of Figure 2A, but no statistical study was performed due to the bias of the orientation of the objects on the substrate). The average diameter of the PS nodules

on bipods is 1350 nm with a polydispersity index of 1.13, higher than that of the silica seeds. The by-products are mainly monopods (5%), tripods (13%) and objects combining several silica seeds or with uncertain morphology (13%). A few PS particles independent of any silica seed can also be observed, but without any consequence on the following steps, since they are spontaneously eliminated when the PS is dissolved. Regardless of the object concerned, the average size of all PS nodules is 1375 nm (PDI = 1.06). Thus the wider size distribution of the bipod nodules confirms that they are the result of coalescence reactions as they grow on the silica seeds [20,21].

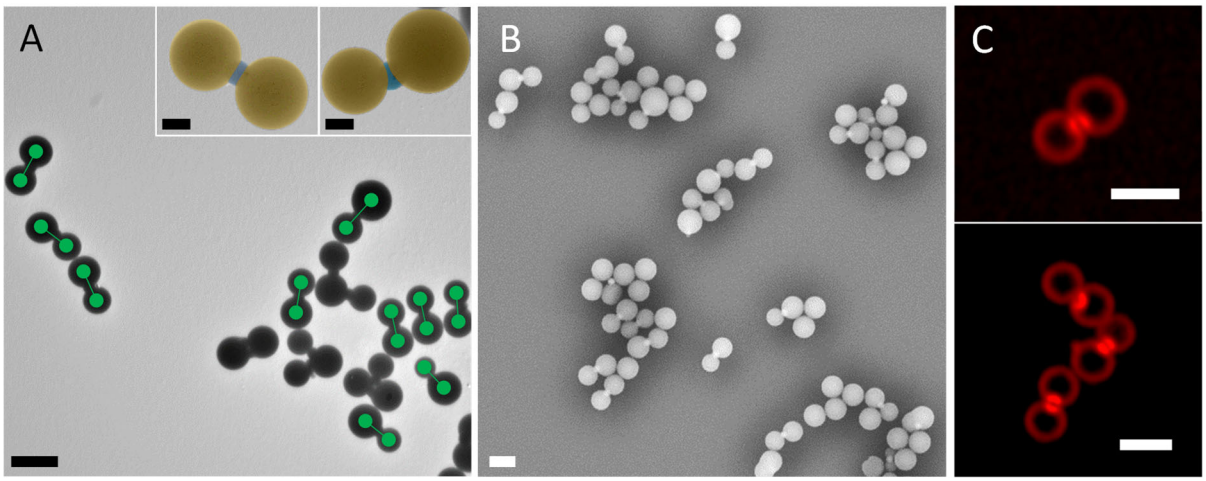

Figure 2: Representative images of silica/PS bipods obtained from 500-nm silica seeds by dispersion polymerisation of styrene. A) Transmission electron microscopy image where particles unmistakably recognised as bipods are marked in green (Insets: artificially colourised images showing a regular bipod and a bent bipod). B) Scanning electron microscopy image. C) Fluorescence confocal images under excitation at 488 nm. Scale bars: 2 µm (500 nm in the insets).

We also studied the bipods under a confocal fluorescence microscope after they had been labelled with Nile red, a hydrophobic staining agent (Figure 2C). The focal plane was adjusted to pass through the centres of the three spheres that make up the object, so this is a cross-section of the bipod. One can see that Nile red specifically marked the hydrophobic surface of the PS nodules suggesting that the PS does not cover the silica surface between the nodules. A counter-experiment, not shown here, was to verify that the polysiloxane film on the surface of the silica seeds is not labelled by Nile red under these conditions.

3.2 Conversion of silica/PS bipods to two-patch silica particles

The PS nodules were dissolved during successive washing steps in tetrahydrofuran. This step aimed to eliminate only physically entangled macromolecules and to keep only those covalently bound to the surface of the silica particles. The number-average and mass-average molar masses of the extracted macromolecules analysed by size exclusion chromatography are M_n = 110,000 g/mol and M_w = 200,000 g/mol, respectively. It is generally accepted that the molar masses of the grafted chains are of the same order of magnitude as those extracted [25].

TEM analysis of the bipods after THF treatment shows that the particles are again quasi-spherical objects with a diameter of 500 nm corresponding to that of the initial silica seeds (Figure 3A-D). Close

examination of the periphery of the particles shows the presence of a discontinuous 10-20 nm excess thickness whose lower electron beam absorption indicates that it was a film of organic nature. By comparing with the TEM images before dissolution (Insets of Figure 2A), we can see that the widths of the free spaces between the nodules, on the one hand, and of the areas between the organic films, on the other hand, are approximately similar: about 100 to 120 nm (approximate values, however, because the measurements are dependent on the orientation of the particles with respect to the electron beam). This experiment thus seems to confirm the hypothesis that the organic overthicknesses correspond to the locations of the PS nodules. By observing more than twenty particles, we were able to find at least three that were sufficiently well oriented on the TEM grid to allow us to reconstruct the two grafted polystyrene patches (Figure 3A-C) as well as a fourth particle where the position of the organic films suggests that it was a three-patch particle, as the tripods were present up to 13% in the initial batch (Figure 3D).

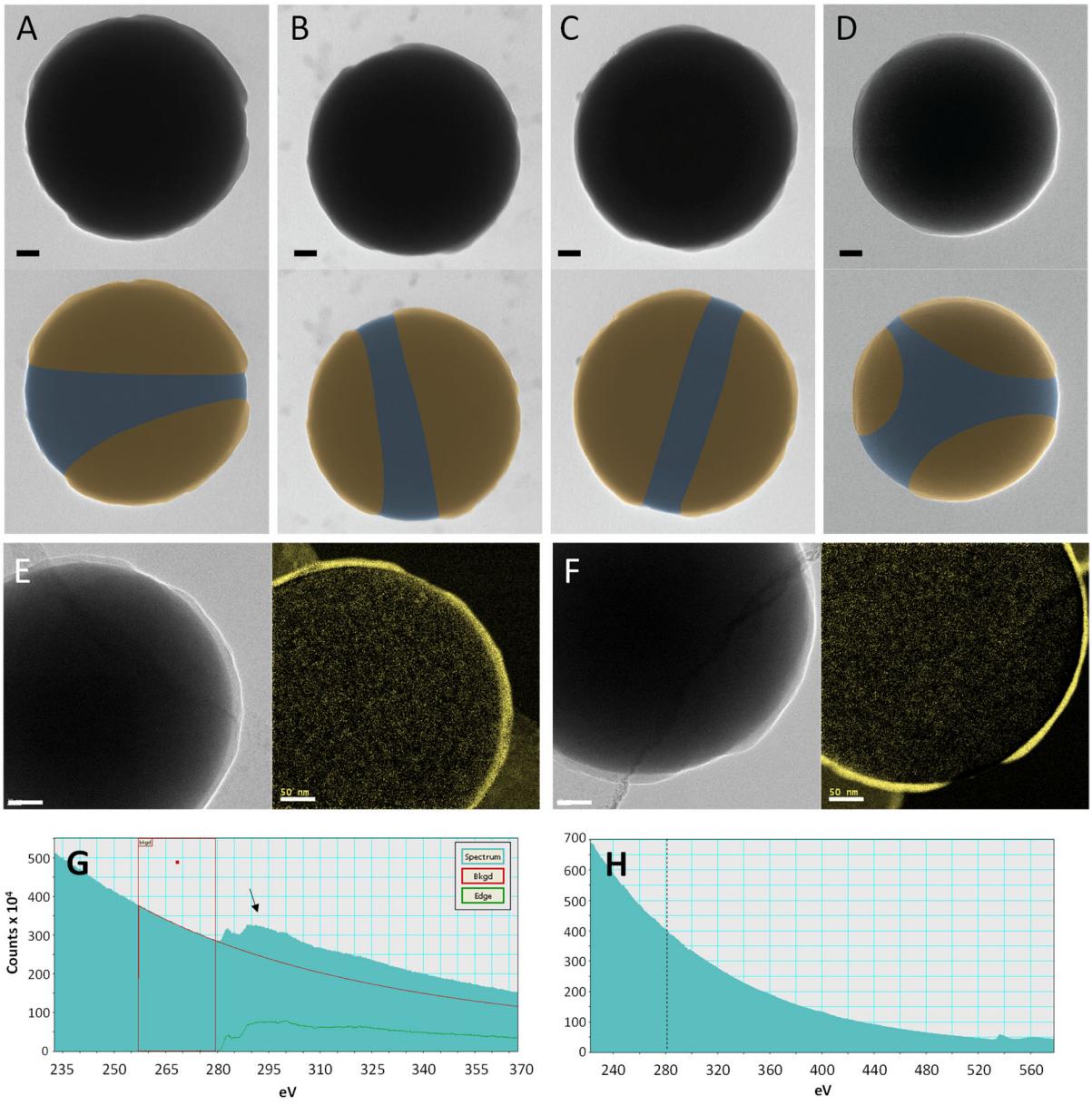

Figure 3: Patchy silica particles obtained after dissolution of the PS nodules of the bipod-like particles. A-D) Representative TEM images of four particles: original images (top) and same images artificially colourised for showing the patch position (bottom). Scale bars: 50 nm. E-F) Representative TEM images and EELS images extracted from the data at the energy of carbon K edge at 284 eV. Scale bars: 50 nm. G-H) Typical EELS spectra showing the carbon K-edge at 284 eV from a zone of the light grey thin layer in Figure F and from the surface of a silica particle before polymerisation, respectively.

To verify that these patches were organic in nature, we analysed their composition by electron energy-loss spectroscopy (EELS). The corresponding TEM images and carbon element maps are shown in Figure 3E-F. These reveal that carbon was largely present in the thicker films and almost absent elsewhere. Furthermore, comparison of the EELS spectrum recorded on the organic patches (Figure 3G) with those determined on the silica seeds before polymerisation (Figure 3H) shows that the amount of carbon detected in the polysiloxane film was very low. Thus, it is plausible that the films observed on the particles consisted of grafted PS macromolecules, and corresponded to the permanent residues of the PS nodules. We have thus demonstrated that it is possible to create patchy particles from silica/PS bipods obtained by dispersion polymerisation.

The use of PEI as a stabiliser in the seeded-growth dispersion polymerisation for the synthesis of bipods appears to be a key requirement for the formation of patches. Indeed, we performed experiments using PVP more conventionally. A control experiment where we simply replaced PEI with PVP did not lead to the formation of bipods, but monopods with a record morphological purity of 99% (Figure S1). This proves that the stabilising properties of PVP and PEI are different. To obtain bipods from the PVP recipe, we had to modify the experimental conditions, in particular starting from a silica size of 800 nm (see supplementary information for the experimental details, and Figure S2A). The batch of bipods obtained was then 54% pure (Figure S2B). After dissolving the PS and carefully examining the surface by TEM and EELS, we could not detect the presence of patches: the PS layer on the surface seems to be continuous and covers the whole surface (Figure S3). Our hypothesis that could explain this difference would be that PVP is known to undergo chain transfer reactions leading to PS-grafted copolymers explaining its stabilizing power. Such an amphiphilic copolymer could thus adsorb onto the silica surface, making the patches indistinguishable from the inter-patch areas. To our knowledge, the ability of PEI to undergo chain transfer reactions during the polymerisation of styrene has not been reported. Further experiments would certainly be necessary to understand better this difference in behaviour and its origin.

3.3 Purification of the batch of silica/PS bipods by flow cytometry sorting

We experimented with the purification of our bipod batch by flow cytometry, a technique essentially developed to purify specific cell populations. Although the apparatus allows fluorescence-activated cell sorting, we were content with the label-free results obtained using the light scattering measured by two optical detectors. One detector measured the scattering along the path of the laser (forward scattering) while the other measured the scattering at a 90° angle to the laser (sideward scattering). Measuring forward and/or sideward scattering allows objects to be discriminated by size: the larger the volume of a particle the more light it scatters. The measurement of the lateral scattering gives additional information on the internal complexity of the object, *i.e*. its granularity. The combination of these two measurements allows a certain degree of differentiation of objects within a heterogeneous population. Not surprisingly, we found that the amount of scattered light scaled essentially with the amount of PS in each multipod. PS has a much higher refractive index than silica and, as it can be seen

from the SEM pictures (Figure 2), the PS nodules are much larger than the silica cores. The flow containing the characterized multipods was electrically charged and broken up into droplets containing on average less than one particle. Two electrodes were then used to deflect these drops electrostatically into different containers according to the criteria we set for the forward and sideward scattering signals, thus allowing sorting.

We studied the purification of the bipod batch (69% pure) by this flow cytometry method. First, we measured forward scattering (FSC) and side scattering (SSC) to determine the populations to be collected. The populations R4, R3, R2, R1 and R5 (Figure 4) were collected in different tubes. We sorted approximately $3.33*10^8$ objects, with R3 and R2 representing 57% and 32% of the sorted objects, respectively. The objects of the different populations were observed by SEM in order to determine the sorting efficiency (insets of Figure 4). The R4 population (4% of the objects collected) contained mainly micron-sized impurities and was associated with low forward and lateral scattering due to its smaller size with respect to the other particles. The R3 population contained mostly free PS particles and monopods of the order of 1400 nm. Bipods twice the size of monopods were present in the R2 population and it was observed that the forward scattering was effectively doubled. The R1 and R5 populations with more forward scattering contained the asymmetric bipods as well as the tripods. The bipods were collected in the R2 area and their purity was estimated at 98% (statistical analysis made over 200 particles).

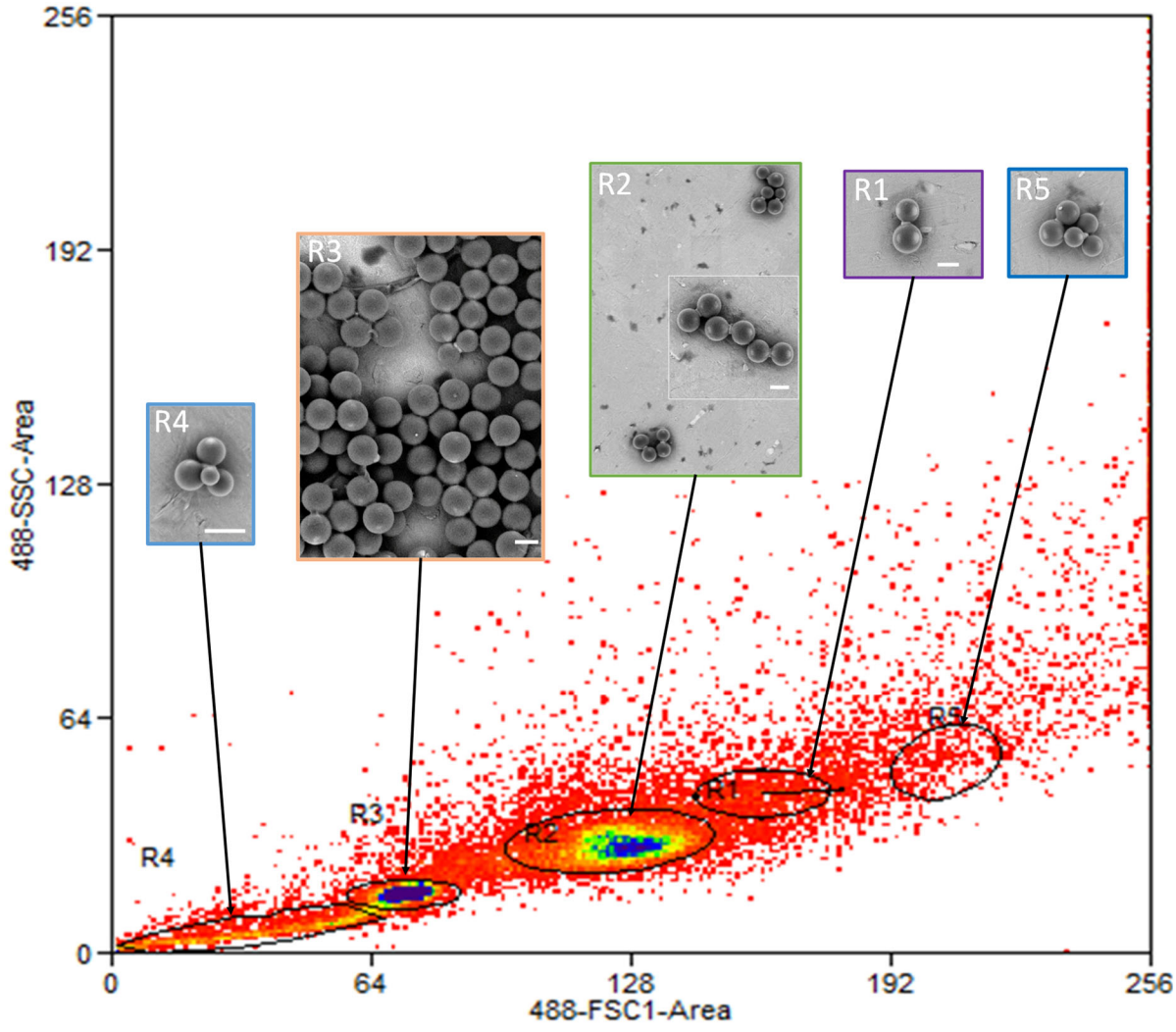

Figure 4: Representative scatter plot of the bipod batch from the software of the Beckman Coulter flow cytometer giving the area of the forward scattering peaks of the 488 nm laser (488-FSC1-Area) vs the area of the sideward scattering peaks (488-SSC-Area) in false colours that represent the number of observations, with the set fractionation regions in black and SEM views of the collected populations. Scale bars: 1 μm.

4. Conclusions

In summary, this work demonstrated that silica/PS bipods can be obtained by dispersion polymerization using PEI as stabiliser. Their morphological purity reached ~70%. To the best of our knowledge, this is the first report of the use of flow cytometry sorting to purify patchy particles. By doing so, the purity of the bipods could be increased up to 98%. After the specific dissolution of the PS nodules of the bipods, a careful analysis by TEM combined with EELS revealed the formation of silica particles bearing two organic patches by the grafted PS chains. The PEI stabiliser seems to play a role in this success, as we did not achieve the same observation with particles made in the presence of PVP.

By comparison with previously reported methods such as stamping or glancing angle deposition, which allow to produce small quantities of 2-patch particles, our strategy gives access to samples at the gram scale. We anticipate these results open up avenues to construct new colloidal building units, such as, for instance, inverse patchy particles [26] for the programmed assembly of new structures with photonic or catalytic properties [27,28]. For instance, the functionalization of the organic patches with azide groups would enable us to graft dibenzocyclooctyne-terminated DNA strands [29], opening the way to the synthesis of colloidal chains with predetermined sequence and colloidal crystals with well-defined architecture.

Acknowledgements

We acknowledge Emanuela Bianchi from the TU Wien for her contribution to the bi-lateral ANR-FWF project I 3577-N28 that co-financed this research. Some of the TEM experiments and the EELS characterizations were performed at the Plateforme de Caractérisation des Matériaux (UAR CNRS 3626) at the university of Bordeaux. Some of the SEM experiments were performed at the Apreo VS SEM (Thermo Scientific, Eindhoven, The Netherlands) (Vienna). We gratefully acknowledge Valentin Maingret and Vaïana Royer (LCPO, Pessac) for having performed the SEC experiments and Konstantin Beitl for help with the recording of images with the SEM in Vienna.

Funding

This work was carried out in the context of the HotCHPot project co-funded by the French agency for research (ANR-17-CE09-0048).

References

[1] S. Ravaine, E. Duguet, Synthesis and assembly of patchy particles: Recent progress and future prospects, Curr. Opin. Colloid Interface Sci. 30 (2017) 45–53. doi:10.1016/j.cocis.2017.05.002.

[2] W. Li, H. Palis, R. Mérindol, J. Majimel, S. Ravaine, E. Duguet, Colloidal molecules and patchy particles: complementary concepts, synthesis and self-assembly, Chem. Soc. Rev. 49 (2020) 1955–1976. doi:10.1039/C9CS00804G.

[3] Q. Chen, S.C. Bae, S. Granick, Staged self-assembly of colloidal metastructures, J. Am. Chem. Soc. 134 (2012) 11080–11083. doi:10.1021/ja303434d.

[4] Z. Nie, D. Fava, E. Kumacheva, S. Zou, G.C. Walker, M. Rubinstein, Self-assembly of metal–polymer analogues of amphiphilic triblock copolymers, Nat. Mater. 6 (2007) 609–614. doi:10.1038/nmat1954.

[5] W. Li, B. Liu, C. Hubert, A. Perro, E. Duguet, S. Ravaine, Self-assembly of colloidal polymers from two-patch silica nanoparticles, Nano Res. 13 (2020) 3371–3376. doi:10.1007/s12274-020-3024-1.

[6] B. Liu, W. Li, E. Duguet, S. Ravaine, Linear assembly of two-patch silica nanoparticles and control of chain length by coassembly with colloidal chain stoppers, ACS Macro Lett. 11 (2022) 156–160. doi:10.1021/acsmacrolett.1c00699.

[7] Q. Chen, S.C. Bae, S. Granick, Directed self-assembly of a colloidal kagome lattice, Nature. 469 (2011) 381–384. doi:10.1038/nature09713.

[8] A.B. Pawar, I. Kretzschmar, Multifunctional patchy particles by glancing angle deposition, Langmuir. 25 (2009) 9057–9063. doi:10.1021/la900809b.

[9] P.D.J. van Oostrum, M. Hejazifar, C. Niedermayer, E. Reimhult, Simple method for the synthesis of inverse patchy colloids, J. Phys. Condens. Matter. 27 (2015) 234105. doi:10.1088/0953-8984/27/23/234105.

[10] M. Zimmermann, D. Grigoriev, N. Puretskiy, A. Böker, Characteristics of microcontact printing with polyelectrolyte ink for the precise preparation of patches on silica particles, RSC Adv. 8 (2018) 39241–39247. doi:10.1039/C8RA07955B.

[11] S. Reculusa, C. Poncet-Legrand, S. Ravaine, C. Mingotaud, E. Duguet, E. Bourgeat-Lami, Syntheses of raspberrylike silica/polystyrene materials, Chem. Mater. 14 (2002) 2354–2359. doi:10.1021/cm0116525.

[12] J. Hong, J. Lee, Y.-M. Rhym, D.-H. Kim, S.E. Shim, Polyelectrolyte-assisted synthesis of polystyrene microspheres by dispersion polymerization and the subsequent formation of silica shell, J. Colloid Interface Sci. 344 (2010) 410–416. doi:10.1016/j.jcis.2010.01.001.

[13] A. Schmid, S. Fujii, S.P. Armes, C.A.P. Leite, F. Galembeck, H. Minami, N. Saito, M. Okubo, Polystyrene-silica colloidal nanocomposite particles prepared by alcoholic dispersion polymerization, Chem. Mater. 19 (2007) 2435–2445. doi:10.1021/cm062314c.

[14] A. Schmid, S. Fujii, S.P. Armes, Synthesis of micrometer-sized silica-stabilized polystyrene latex particles, Langmuir. 21 (2005) 8103–8105. doi:10.1021/la051687+.

[15] A. Schmid, S. Fujii, S.P. Armes, Polystyrene−silica nanocomposite particles via alcoholic dispersion polymerization using a cationic azo initiator, Langmuir. 22 (2006) 4923–4927. doi:10.1021/la060308p.

[16] A. Schmid, J. Tonnar, S.P. Armes, A new highly efficient route to polymer-silica colloidal nanocomposite particles, Adv. Mater. 20 (2008) 3331–3336. doi:10.1002/adma.200800506.

[17] K. Yoshinaga, T. Yokoyama, Y. Sugawa, H. Karakawa, N. Enomoto, H. Nishida, M. Komatsu, Preparation of monodispersed polymer-modified silica particles by radical polymerization using silica colloid and introduction of functional groups on the composite surface, Polym. Bull. 28 (1992) 663–668. doi:10.1007/BF00295970.

[18] E. Bourgeat-Lami, J. Lang, Encapsulation of inorganic particles by dispersion polymerization in polar media. Part 1 - Silica nanoparticles encapsulated by polystyrene, J. Colloid Interface Sci. 197 (1998) 293–308. doi:10.1006/jcis.1997.5265.

[19] E. Bourgeat-Lami, J. Lang, Encapsulation of inorganic particles by dispersion polymerization in polar media. Part 2 - Effect of silica size and concentration on the morphology of silica-polystyrene composite particles, J. Colloid Interface Sci. 210 (1999) 281–289. doi:10.1006/jcis.1998.5939.

[20] D. Nguyen, E. Duguet, E. Bourgeat-Lami, S. Ravaine, An easy way to control the morphology of colloidal polymer-oxide supraparticles through seeded dispersion polymerization, Langmuir. 26 (2010) 6086–6090. doi:10.1021/la100357q.

[21] D. Nguyen, S. Ravaine, E. Bourgeat-Lami, E. Duguet, About the suitability of the seeded-dispersion polymerization technique for preparing micron-sized silica-polystyrene clusters, J. Mater. Chem. 20 (2010) 9392–9400. doi:10.1039/b926438h.

[22] Z. Zhang, H. Shao, X. Zhou, L. Zhao, H. Liu, X. Ji, H. Liu, Controllable synthesis of anisotropic silica/polymer composite particles via seeded dispersion polymerization, Mater. Chem. Phys. 195 (2017) 105–113. doi:10.1016/j.matchemphys.2017.04.024.

[23] A. Cossarizza, H. Chang, A. Radbruch, A. Acs, D. Adam, S. Adam-Klages, W.W. Agace, N. Aghaeepour, M. Akdis, M. Allez, L.N. Almeida, G. Alvisi, G. Anderson, I. Andrä, F. Annunziato, A. Anselmo, P. Bacher, C.T. Baldari, S. Bari, V. Barnaba, J. Barros-Martins, L. Battistini, W. Bauer, S. Baumgart, N. Baumgarth, D. Baumjohann, B. Baying, M. Bebawy, B. Becher, W. Beisker, V. Benes, R. Beyaert, A. Blanco, D.A. Boardman, C. Bogdan, J.G. Borger, G. Borsellino, P.E. Boulais, J.A. Bradford, D. Brenner, R.R. Brinkman, A.E.S. Brooks, D.H. Busch, M. Büscher, T.P. Bushnell, F. Calzetti, G. Cameron, I. Cammarata, X. Cao, S.L. Cardell, S. Casola, M.A. Cassatella, A. Cavani, A. Celada, L. Chatenoud, P.K. Chattopadhyay, S. Chow, E. Christakou, L. Čičin-Šain, M. Clerici, F.S. Colombo, L. Cook, A. Cooke, A.M. Cooper, A.J. Corbett, A. Cosma, L. Cosmi, P.G. Coulie, A. Cumano, L. Cvetkovic, V.D. Dang, C. Dang-Heine, M.S. Davey, D. Davies, S. De Biasi, G. Del Zotto, G.V. Dela Cruz, M. Delacher, S. Della Bella, P. Dellabona, G. Deniz, M. Dessing, J.P. Di Santo, A. Diefenbach, F. Dieli, A. Dolf, T. Dörner, R.J. Dress, D. Dudziak, M.

Dustin, C. Dutertre, F. Ebner, S.B.G. Eckle, M. Edinger, P. Eede, G.R.A. Ehrhardt, M. Eich, P. Engel, B. Engelhardt, A. Erdei, C. Esser, B. Everts, M. Evrard, C.S. Falk, T.A. Fehniger, M. Felipo-Benavent, H. Ferry, M. Feuerer, A. Filby, K. Filkor, S. Fillatreau, M. Follo, I. Förster, J. Foster, G.A. Foulds, B. Frehse, P.S. Frenette, S. Frischbutter, W. Fritzsche, D.W. Galbraith, A. Gangaev, N. Garbi, B. Gaudilliere, R.T. Gazzinelli, J. Geginat, W. Gerner, N.A. Gherardin, K. Ghoreschi, L. Gibellini, F. Ginhoux, K. Goda, D.I. Godfrey, C. Goettlinger, J.M. González-Navajas, C.S. Goodyear, A. Gori, J.L. Grogan, D. Grummitt, A. Grützkau, C. Haftmann, J. Hahn, H. Hammad, G. Hämmerling, L. Hansmann, G. Hansson, C.M. Harpur, S. Hartmann, A. Hauser, A.E. Hauser, D.L. Haviland, D. Hedley, D.C. Hernández, G. Herrera, M. Herrmann, C. Hess, T. Höfer, P. Hoffmann, K. Hogquist, T. Holland, T. Höllt, R. Holmdahl, P. Hombrink, J.P. Houston, B.F. Hoyer, B. Huang, F. Huang, J.E. Huber, J. Huehn, M. Hundemer, C.A. Hunter, W.Y.K. Hwang, A. Iannone, F. Ingelfinger, S.M. Ivison, H. Jäck, P.K. Jani, B. Jávega, S. Jonjic, T. Kaiser, T. Kalina, T. Kamradt, S.H.E. Kaufmann, B. Keller, S.L.C. Ketelaars, A. Khalilnezhad, S. Khan, J. Kisielow, P. Klenerman, J. Knopf, H. Koay, K. Kobow, J.K. Kolls, W.T. Kong, M. Kopf, T. Korn, K. Kriegsmann, H. Kristyanto, T. Kroneis, A. Krueger, J. Kühne, C. Kukat, D. Kunkel, H. Kunze-Schumacher, T. Kurosaki, C. Kurts, P. Kvistborg, I. Kwok, J. Landry, O. Lantz, P. Lanuti, F. LaRosa, A. Lehuen, S. LeibundGut-Landmann, M.D. Leipold, L.Y.T. Leung, M.K. Levings, A.C. Lino, F. Liotta, V. Litwin, Y. Liu, H. Ljunggren, M. Lohoff, G. Lombardi, L. Lopez, M. López-Botet, A.E. Lovett-Racke, E. Lubberts, H. Luche, B. Ludewig, E. Lugli, S. Lunemann, H.T. Maecker, L. Maggi, O. Maguire, F. Mair, K.H. Mair, A. Mantovani, R.A. Manz, A.J. Marshall, A. Martínez-Romero, G. Martrus, I. Marventano, W. Maslinski, G. Matarese, A.V. Mattioli, C. Maueröder, A. Mazzoni, J. McCluskey, M. McGrath, H.M. McGuire, I.B. McInnes, H.E. Mei, F. Melchers, S. Melzer, D. Mielenz, S.D. Miller, K.H.G. Mills, H. Minderman, J. Mjösberg, J. Moore, B. Moran, L. Moretta, T.R. Mosmann, S. Müller, G. Multhoff, L.E. Muñoz, C. Münz, T. Nakayama, M. Nasi, K. Neumann, L.G. Ng, A. Niedobitek, S. Nourshargh, G. Núñez, J. O'Connor, A. Ochel, A. Oja, D. Ordonez, A. Orfao, E. Orlowski-Oliver, W. Ouyang, A. Oxenius, R. Palankar, I. Panse, K. Pattanapanyasat, M. Paulsen, D. Pavlinic, L. Penter, P. Peterson, C. Peth, J. Petriz, F. Piancone, W.F. Pickl, S. Piconese, M. Pinti, A.G. Pockley, M.J. Podolska, Z. Poon, K. Pracht, I. Prinz, C.E.M. Pucillo, S.A. Quataert, L. Quatrini, K.M. Quinn, H. Radbruch, T.R.D.J. Radstake, S. Rahmig, H. Rahn, B. Rajwa, G. Ravichandran, Y. Raz, J.A. Rebhahn, D. Recktenwald, D. Reimer, C. Reis e Sousa, E.B.M. Remmerswaal, L. Richter, L.G. Rico, A. Riddell, A.M. Rieger, J.P. Robinson, C. Romagnani, A. Rubartelli, J. Ruland, A. Saalmüller, Y. Saeys, T. Saito, S. Sakaguchi, F. Sala-de-Oyanguren, Y. Samstag, S. Sanderson, I. Sandrock, A. Santoni, R.B. Sanz, M. Saresella, C. Sautes-Fridman, B. Sawitzki, L. Schadt, A. Scheffold, H.U. Scherer, M. Schiemann, F.A. Schildberg, E. Schimisky, A. Schlitzer, J. Schlosser, S. Schmid, S. Schmitt, K. Schober, D. Schraivogel, W. Schuh, T. Schüler, R. Schulte, A.R. Schulz, S.R. Schulz, C. Scottá, D. Scott-Algara, D.P. Sester, T.V. Shankey, B. Silva-Santos, A.K. Simon, K.M. Sitnik, S. Sozzani, D.E. Speiser, J. Spidlen, A. Stahlberg, A.M. Stall, N. Stanley, R. Stark, C. Stehle, T. Steinmetz, H. Stockinger, Y. Takahama, K. Takeda, L. Tan, A. Tárnok, G. Tiegs, G. Toldi, J. Tornack, E. Traggiai, M. Trebak, T.I.M. Tree, J. Trotter, J. Trowsdale, M. Tsoumakidou, H. Ulrich, S. Urbanczyk, W. Veen, M. Broek, E. Pol, S. Van Gassen, G. Van Isterdael, R.A.W. Lier, M. Veldhoen, S. Vento-Asturias, P. Vieira, D. Voehringer, H. Volk, A. Borstel, K. Volkmann, A. Waisman, R. V. Walker, P.K. Wallace, S.A. Wang, X.M. Wang, M.D. Ward, K.A. Ward-Hartstonge, K. Warnatz, G. Warnes, S. Warth, C. Waskow, J. V. Watson, C. Watzl, L. Wegener, T. Weisenburger, A. Wiedemann, J. Wienands, A. Wilharm, R.J. Wilkinson, G. Willimsky, J.B. Wing, R. Winkelmann, T.H. Winkler, O.F. Wirz, A. Wong, P. Wurst, J.H.M. Yang, J. Yang, M. Yazdanbakhsh, L. Yu, A. Yue, H. Zhang, Y. Zhao, S.M. Ziegler, C. Zielinski, J. Zimmermann, A. Zychlinsky, Guidelines for the use of flow cytometry and cell sorting in immunological studies (second edition), Eur. J. Immunol. 49 (2019) 1457–1973. doi:10.1002/eji.201970107.

[24] M. Abboud, M. Turner, E. Duguet, M. Fontanille, PMMA-based composite materials with reactive ceramic fillers. Part 1.—Chemical modification and characterisation of ceramic

particles, J. Mater. Chem. 7 (1997) 1527. doi:10.1039/a700573c.

[25] C. Chomette, E. Duguet, S. Mornet, E. Yammine, V.N. Manoharan, N.B. Schade, C. Hubert, S. Ravaine, A. Perro, M. Tréguer-Delapierre, Templated growth of gold satellites on dimpled silica cores, Faraday Discuss. 191 (2016) 105–116. doi:10.1039/C6FD00022C.

[26] E. Bianchi, P.D.J. van Oostrum, C.N. Likos, G. Kahl, Inverse patchy colloids: Synthesis, modeling and self-organization, Curr. Opin. Colloid Interface Sci. 30 (2017) 8–15. doi:10.1016/j.cocis.2017.03.010.

[27] S. Ferrari, E. Bianchi, G. Kahl, Spontaneous assembly of a hybrid crystal-liquid phase in inverse patchy colloid systems, Nanoscale. 9 (2017) 1956–1963. doi:10.1039/C6NR07987C.

[28] E.G. Noya, I. Kolovos, G. Doppelbauer, G. Kahl, E. Bianchi, Phase diagram of inverse patchy colloids assembling into an equilibrium laminar phase, Soft Matter. 10 (2014) 8464–8474. doi:10.1039/C4SM01559B.

[29] T. Zhang, D. Lyu, W. Xu, Y. Mu, Y. Wang, Programming self-assembled materials with DNA-coated colloids, Front. Phys. 9 (2021) 1–17. doi:10.3389/fphy.2021.672375.

Graphical abstract